A Model for Ice Accretion Roughness Evolution and Spatial Variations

Stephen T. McClain[1]
Baylor University, Waco, TX 76798-7356

Mario Vargas[2]
NASA Glenn Research Center, Cleveland, OH 44135

Jen-Ching Tsao[3]
Ohio Aerospace Institute, Cleveland, OH 44142

and

Andy P. Broeren[4]
NASA Glenn Research Center, Cleveland, OH 44135

Over the past decade, multiple investigations of ice accretion roughness and spatial variations have been performed in the Icing Research Tunnel (IRT) at the NASA Glenn Research Center. The early investigations used models of NACA 0012 airfoils with different chord sizes and focused on temporal scaling and primary cloud scaling parameters such as stagnation point collection efficiency. Subsequent investigations included the effects of model sweep, airfoil shape, airfoil lifting condition, and freestream static temperature. To develop a predictive model for roughness evolution in generalized icing situations, the maximum roughness values for the airfoils and conditions used in the angle of attack and freestream temperature investigations were scaled to eliminate the temporal variations. LEWICE simulations were employed to identify the local collection efficiency at the locations of maximum roughness, and a two-dimensional panel-method code was used to identify the local static pressure at the location of the maximum roughness. Because of the stochastic nature of ice accretion roughness, a physics-directed approach was employed to develop a multi-dimensional correlation based on the local pressure coefficient, the local total temperature, the cloud properties, and the cloud exposure time. The resulting correlation predictions are compared to ice shapes measured in the IRT for both a 21-in. NACA 0012 airfoil model and a 60-in. HAARP-II model. The resulting predictions indicate that the local freezing fraction must be included in the roughness predictive model. Implications regarding icing heat transfer predictions using the resulting roughness model are also discussed.

Nomenclature

A_c	=	Accumulation parameter
$\boldsymbol{b_n}$	=	Codebook vector used to represent mean ice shape
AOA	=	Angle of attack
C_L	=	Lift coefficient
c_p	=	Specific heat of air
$c_{p,ws}$	=	Specific heat of water at the surface temperature
d_0	=	Leading-edge diameter

[1] Professor, Department of Mechanical Engineering, One Bear Place #97356, AIAA Associate Fellow.
[2] Aerospace Engineer, Icing Branch, 21000 Brookpark Rd., MS 11-2, AIAA Associate Fellow.
[3] Principal Research Scientist, Icing Branch, 21000 Brookpark Rd., MS 11-2, AIAA Associate Fellow.
[4] Aerospace Engineer, Icing Branch, 21000 Brookpark Rd., MS 11-2, AIAA Associate Fellow.

h_c	=	Convective heat transfer coefficient
h_G	=	Convective mass transfer coefficient
K	=	droplet inertial parameter
LWC	=	Liquid water content [gm/m^3]
M_∞	=	Mach number of freestream flow
MVD	=	Median volumetric diameter [μm]
N	=	Airfoil or mean ice shape surface normal coordinate direction
$N_{0,R}$	=	Fully-dense (ideal) rime ice stagnation thickness on an unswept wing ($\Lambda = 0°$) at the stagnation point
$N_{L,R}$	=	Local fully-dense (ideal) rime ice stagnation thickness at a point on airfoil surface
$N_{\Lambda,R}$	=	Fully-dense (ideal) rime ice surface-orthogonal thickness on swept wings at the attachment line
$\overline{N}_0$	=	The measured ice orthogonal-thickness at each codebook vector relative to the clean wing surface
n	=	Local freezing fraction
n_0	=	Stagnation point freezing fraction
P_{st}	=	Static pressure
P_{tot}	=	Total pressure
P_w	=	Vapor pressure of water vapor
P_{ww}	=	Vapor pressure of water vapor at the icing surface
RMH	=	99%-Gaussian roughness maximum height evaluated at each codebook vector (=3.09R_q)
R_q	=	Root-mean-square or "standard deviation" roughness height
r_0	=	Leading-edge radius of curvature
S	=	Mean ice shape surface tangential coordinate direction
S_0	=	Clean airfoil tangential coordinate direction and distance
SEE	=	Standard error of the estimate
SOM	=	Self-Organizing Map
T_s	=	Surface temperature
T_f	=	Freezing temperature of water
T_{st}	=	Freestream static temperature
T_{tot}	=	Freestream stagnation or total temperature
V or U_∞	=	Freestream velocity
x_s	=	Roughness height scaled relative to the leading-edge diameter
β_S	=	Local surface collection efficiency at a point on the surface
β_0	=	Straight wing stagnation collection efficiency
Δt_s	=	Spray or ice accretion event time
Λ	=	Sweep angle
Λ_f	=	Latent heat of freezing of water
Λ_v	=	Latent heat of vaporization of water
ρ_{ice}	=	Density of ice
ρ_w	=	Density of liquid water
μ_{air}	=	Viscosity of air

I. Introduction

PREDICTING the convective heat transfer augmentation of a rough ice accretion surface is a critical feature of any ice accretion modeling code. The local convection rates determine the fraction of the water existing along a surface that solidifies for each time increment of the ice accretion process. To make good predictions of the roughness convective enhancement, modeling codes must be able to predict the magnitude of ice roughness at each location along the simulated surface.

In the convection model used in LEWICE [1], which is an ice accretion modeling code created and maintained by NASA, only the maximum roughness is predicted based on the stagnation point freezing fraction (n_0). The predicted maximum roughness used in LEWICE, which is scaled using the leading edge-diameter, is shown in Eq. (1).

$$x_s = \frac{1}{2}\sqrt{0.15 + \frac{0.3}{n_0}} \tag{1}$$

The maximum equivalent sand-grain roughness height then calculated using Eq. (2).

$$k_s = x_s d_0 \tag{2}$$

The resulting maximum equivalent sand-grain roughness value calculated from Eq. (2) is applied over the entire ice accretion simulation domain and is held constant during the simulation.

Shannon and McClain [2] used flow and convection measurements from unwrapped ice accretion surfaces to investigate each aspect of the LEWICE roughness convective enhancement model. Shannon and McClain [2] found that while the roughness model used in LEWICE overestimates the roughness height for most of the early icing process, the LEWICE model gets the maximum roughness value correct as the ice shape transitions from ice roughness to a substantial ice accretion that results in aerodynamic changes of the airfoil shape. The skin friction modeling approach used in LEWICE also overestimates the resulting surface shear values on the surface. The overestimates of the roughness size and local skin friction coefficient are then corrected by the use of the convection correlation of Kays and Crawford [3].

Since 2014, multiple studies have been performed in the Icing Research Tunnel at NASA Glenn Research Center to better understand and model ice accretion roughness evolution and spatial variations. The early investigations [4, 5] were on a 53.34-cm (21-in.) NACA 0012 at 0° angle of attack. The symmetric airfoil at 0° angle of attack is a configuration commonly employed for icing investigations because the aerodynamic performance has been investigated many times and is relatively well understood. The efforts reported in Ref. 4 and 5 focused on replication the conditions used in the investigations of Anderson et al. [6]. The investigations of McClain et al. [7] and McClain et al. [8] introduced a 72-in. NACA 0012 and a 36-in. NACA 0012 with a sweep angle of 30° to begin investigations of scaling properties relative to cloud and icing physics.

Recently, McClain et al. [9-11] published roughness results using the HAARP-II airfoil model, which was developed for the Hot Air Anti-Icing Research Program performed during the mid-2000's [15]. The HAARP-II airfoil was developed to simulate the performance of business jet wings. Additionally, the HAARP-II airfoil has geometric features similar to the supercritical wing geometry expected for the D8-Double Bubble aircraft developed for NASA's Advanced Air Transport Technology (AATT) Project of the Advanced Air Vehicles Program [13], in that the HAARP-II has a flat upper (extrados) surface and has an aft cusp on its lower (intrados) surface.

In McClain et al. [9] and McClain et al. [10], the results presented were for the HAARP-II model with a -1.9° angle of attack, which is the zero-lift angle of attack for the airfoil. In studying cases at the zero-lift angle attack, the prior HAARP-II investigations focused on the effects of droplet collection efficiency along the surface of the airfoil without the presence of circulation-induced pressure variations along the surface. Using the zero-lift angle of attack also allowed for a consistent comparison to the prior NACA 0012 studies conducted at the zero-lift angle of attack (0°). The investigation of McClain et al. [10] included the variation of the freestream static temperature in its effects on ice accretion roughness. Finally, McClain et al. [11] further included the effects of airfoil angle of attack on the ice accretion roughness evolution and spatial variations.

McClain et al. [11] presented a correlation that included the physics from the prior NACA 0012 and HAARP-II model icing investigations: icing event time, cloud collection efficiency, thermodynamics associated with cloud temperature, and airfoil lifting condition. However, the form of the correlation provided was constructed based on airfoil global and stagnation point conditions, and similarly to the current LEWICE correlation, focused on the maximum roughness that would exist on the airfoil or wing surface. Since ice may accrete on surfaces other than just wings, such as propellers, engine cowlings, and engine compressor components, a more generalized approach to predicting local ice accretion roughness is desired.

In this investigation, the results of McClain et al. [10] and McClain et al. [11] are revisited. LEWICE simulations are used to identify local cloud capture quantities and icing thermodynamic quantities, while a panel method solver is used to predict local surface pressure coefficients. The maximum roughness values along the airfoil models for the NACA 0012 and HAARP-II models employed by McClain et al. [10] and McClain et al. [11] and the predicted local icing and aerodynamic quantities are then used to develop new generalized ice accretion roughness correlation. Finally, the new correlation is applied to specific cases presented in McClain et al. [11] to further investigate the global performance of the correlation over an airfoil surface.

II. Traditional Leading-Edge Ice Roughness Scaling Parameters

Prior roughness modeling efforts on two-dimensional, unswept models have focused on scaling based on the droplet capture and freezing fraction calculations at the stagnation point on the airfoil. The temporal scaling has been related to the exposure time of the aircraft surface in a supercooled cloud and the local collection efficiency. Following the development of Anderson and Tsao [14] and Ruff [15], when the length scale employed in the Stokes number definition is the leading edge radius of the airfoil, the result is commonly referred to in the icing literature as the droplet inertial parameter, K:

$$K = \frac{\rho_w U_\infty MVD^2}{36\mu_{air} r_0} \tag{3}$$

To maintain droplet trajectory similarity, the Langmuir and Blodgett [16] stagnation point collection efficiency, β_0, is employed where

$$\beta_0 = \frac{1.4\left(K_0 - \frac{1}{8}\right)^{0.84}}{1 + 1.4\left(K_0 - \frac{1}{8}\right)^{0.84}} \tag{4}$$

In Eq. (4), K_0 is the modified inertial parameter of Langmuir and Blodgett [16], defined as

$$K_0 = \frac{1}{8} + \frac{\lambda}{\lambda_{Sk}}\left(K - \frac{1}{8}\right) \tag{5}$$

where the parameter λ/λ_{Sk} is the droplet range parameter and is defined as a function of the droplet Reynolds number, $\mathrm{Re}_\delta = \rho V\ MVD/\mu$, as

$$\frac{\lambda}{\lambda_{Sk}} = \frac{1}{0.8388 + 0.001483 Re_\delta + 0.01847\sqrt{Re_\delta}} \tag{6}$$

Once the stagnation point collection efficiency is known, the volume of ice impinging an incremental area at the leading edge may be evaluated as

$$dV_{ice} = \frac{LWC \cdot U_\infty \cdot \beta_0 \cdot \Delta t_s}{\rho_{ice}} dA \tag{7}$$

where dA is the incremental area of the surface. Dividing by the incremental area and multiplying by $2r_0/2r_0$ results in what McClain et al. [8] referred to as the leading-edge, fully-dense, theoretical rime ice ($n_0 = 1$) thickness, $N_{0,R}$, for straight wings and airfoils.

$$N_{0,R} = \frac{LWC \cdot U_\infty \cdot \beta_0 \cdot \Delta t_s}{\rho_{ice}} \frac{2r_0}{2r_0} = 2r_0 A_c \beta_0 \tag{8}$$

In Eq. (8), A_c is the accumulation parameter defined as

$$A_c = \frac{LWC \cdot U_\infty \cdot \Delta t_s}{2r_0 \cdot \rho_{ice}} \tag{9}$$

For swept wings with surfaces oblique to the flow, the Rime ice would be expected to spread over the actual surface area compared to the projected area used in Eq. (7). Consequently, the fully-dense, theoretical Rime ice thickness definition of Eq. (8) would be modified as shown in Eq. (10) to represent the swept wing leading-edge "surface-orthogonal" Rime ice thickness, $N_{\Lambda,R}$.

$$N_{\Lambda,R} \approx 2r_0 A_c \beta_0 \cos(\Lambda) \tag{10}$$

As identified in the current LEWICE correlation and further explored by McClain et al. [11], the stagnation point freezing fraction is also critical to the ice roughness scaling process. The freezing fraction is based on an energy balance including the liquid evaporation rate and calculated using Eq. (11) [14].

$$n_0 = \left(\frac{c_{p,ws}}{\Lambda_f}\right)\left(\varphi + \frac{\theta}{b}\right) \tag{11}$$

where

$$\varphi = T_f - T_{st} - \frac{U_\infty^2}{2c_{p,ws}} \tag{12}$$

$$b = \frac{LWC \cdot V \cdot \beta_0 \cdot c_{p,ws}}{h_c} \tag{13}$$

and

$$\theta = \left(T_s - T_{st} - \frac{U_\infty^2}{2c_p}\right) + \frac{h_G}{h_c}\left(\frac{\frac{P_{ww}}{T_{st}} - \frac{P_{tot}}{T_{tot}}\frac{P_w}{P_{st}}}{\frac{1}{0.622}\frac{P_{tot}}{T_{tot}} - \frac{P_{ww}}{T_{st}}}\right)\Lambda_v \tag{14}$$

Based on the traditional ice shape scaling approaches, the format of the correlation for the airfoil maximum roughness suggested by McClain et al. [11] is shown in Eq. (15).

$$k_{s,max} = C_1\left(a + bC_L\frac{S_0}{|S_0|}\right)N_{\Lambda,R}n_0e^{-C_2n_0} \tag{15}$$

The form presented in Eq. (15) includes the ideal stagnation point or attachment line ideal thickness as the cloud exposure time parameter. The stagnation point freezing fraction is included, and the airfoil lift coefficient is included. Finally, the parameter $S_0/|S_0|$ is a directional indicator that indicates whether the maximum roughness location occurs on the top or bottom side of the airfoil and represents the differences in pressure exhibited on the top and bottom surfaces of a lifting airfoil or wing. Values of the constants and coefficients in Eq. (15) were not provided in McClain et al. [11]; however, the values of C_1 = 11.553, C_2 = 5.0, a = 1.7136, and b = 1.4498 are recommended.

III. Evaluation of Local Surface Quantities

To deviate from the global airfoil approach presented in Eq. (15), the investigations of McClain et al. [10], which focused on the influence of freestream temperature on ice accretion roughness, and McClain et al. [11], which investigated the effects of airfoil angle of attack on ice accretion roughness, were revisited. The airfoil models used in both studies were a 53.35-cm (21-in.) NACA 0012 airfoil and a 60-in. HAARP-II airfoil [12]. The profiles of the wind-tunnel models used are shown in Figure 1.

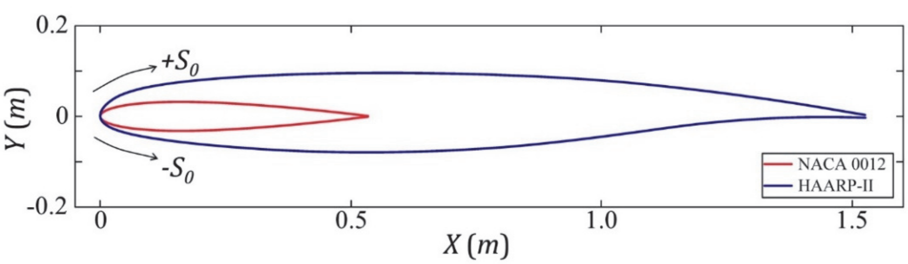

Figure 1. Airfoil Coordinates and Clean Surface Direction Coordinates

The case conditions investigated in McClain et al. [10] and McClain et al. [11] are presented in Tables 1-4. The case conditions were based on the roughness investigations of Anderson et al. [6] and employ basic cloud and speed conditions of MVD = 29.5 µm, LWC = 0.6 gm/m^3, and V = 67 m/s (130 knots). All cases for each of the two studies were performed with accretion event times (spray times) resulting in accumulation parameter values of 0.240.

As shown in Tables 1 and 2, the freestream temperature was changed to progress from a stagnation point freezing fraction of 0.18 to 0.88 for the NACA 0012 with the angle of attack set to 0°. The same freestream temperature cases were performed for the HAARP-II model with an angle of attack of 2.3° resulting in a stagnation point freezing fraction ranging from 0.15 to 0.71.

Tables 3 and 4 show the investigation of McClain et al. [11] is connected to the freestream temperature progression of McClain et al. [10] in that the angle-of attack progressions are performed around "baseline" cases from the temperature progression study. For the NACA 0012, the baseline case stagnation point temperature was -2 °C, (Case 110617.08). For the HAARP-II, the baseline case stagnation point temperature was -2.6 °C, (Case 012517.03). For the angle-of-attack progression, the icing roughness was characterized for the NACA 0012 model using AOA values of 0°, 1.5°, and 3°, while the icing roughness was characterized for the HAARP-II model using AOA values of -1.9°, 0°, 2.3°, and 3°.

Table 1. NACA 0012 Cases for the Freestream Temperature Progression Study of McClain et al. [10]

Case Identifier	AOA (°)	T_{total} (°C)	V (m/s)	MVD (μm)	LWC (gm/m^3)	Δt_s (s)	β_0	A_c	n_0	$N_{A,R}$ (mm)
110617.01	0.0	-1.4	67.0	29.5	0.6	94	0.793	0.240	0.18	3.28
110617.07	0.0	-2.0	67.0	29.5	0.6	94	0.793	0.240	0.23	3.28
110617.02	0.0	-4.2	67.0	29.5	0.6	94	0.793	0.240	0.32	3.28
110617.03	0.0	-5.6	67.0	29.5	0.6	94	0.793	0.240	0.48	3.28
110617.04	0.0	-7.6	67.0	29.5	0.6	94	0.793	0.240	0.62	3.28
110617.05	0.0	-9.7	67.0	29.5	0.6	94	0.793	0.240	0.76	3.28
110617.06	0.0	-11.7	67.0	29.5	0.6	94	0.793	0.240	0.88	3.28

Table 2. HAARP-II Cases for the Freestream Temperature Progression Study of McClain et al. [10]

Case Identifier	AOA (°)	T_{total} (°C)	V (m/s)	MVD (μm)	LWC (gm/m^3)	Δt_s (s)	β_0	A_c	n_0	$N_{A,R}$ (mm)
012617.06	2.3	-1.4	67.0	29.5	0.6	254	0.618	0.240	0.15	6.90
012517.03	2.3	-2.6	67.0	29.5	0.6	254	0.618	0.240	0.22	6.90
012617.07	2.3	-4.2	67.0	29.5	0.6	254	0.618	0.240	0.31	6.90
012617.08	2.3	-5.6	67.0	29.5	0.6	254	0.618	0.240	0.39	6.90
012717.01	2.3	-7.6	67.0	29.5	0.6	254	0.618	0.240	0.50	6.90
012717.02	2.3	-9.7	67.0	29.5	0.6	254	0.618	0.240	0.61	6.90
012717.03	2.3	-11.7	67.0	29.5	0.6	254	0.618	0.240	0.71	6.90

Table 3. NACA 0012 Cases for the AOA Progression Study of McClain et al. [11]

Case Identifier	AOA (°)	T_{total} (°C)	V (m/s)	MVD (μm)	LWC (gm/m^3)	Δt_s (s)	β_0	A_c	n_0	$N_{A,R}$ (mm)
110617.07	0.0	-2.0	67.0	29.5	0.6	94	0.793	0.240	0.22	3.28
110617.08*	1.5	-2.0	67.0	29.5	0.6	94	0.793	0.240	0.22	3.28
110617.09	3.0	-2.0	67.0	29.5	0.6	94	0.793	0.240	0.22	3.28

** Case also appears in Table 1.*

Table 4. HAARP-II Cases for the AOA Progression Study of McClain et al. [11]

Case Identifier	AOA (°)	T_{total} (°C)	V (m/s)	MVD (μm)	LWC (gm/m^3)	Δt_s (s)	β_0	A_c	n_0	$N_{A,R}$ (mm)
012317.03	-1.9	-2.6	67.0	29.5	0.6	254	0.618	0.240	0.22	6.90
012517.07	0.0	-2.6	67.0	29.5	0.6	254	0.618	0.240	0.22	6.90
012517.03*	2.3	-2.6	67.0	29.5	0.6	254	0.618	0.240	0.22	6.90
012717.07	3.0	-2.6	67.0	29.5	0.6	254	0.618	0.240	0.22	6.90

** Case also appears in Table 2.*

The local pressure coefficient, collection efficiency, and the local freezing fraction along the surface of each airfoil was evaluated using either LEWICE or an inviscid panel-method prediction code. LEWICE was used to generate the local collection efficiencies and local freezing fraction values along the surface of each airfoil for the angle of attack progression cases. For each LEWICE simulation, water drop collection efficiencies were calculated using LEWICE version 3.2 [1] for each distinct aerodynamic and icing condition. LEWICE was only run for a single time step in order to compute the drop trajectories, impingement characteristics and freezing fraction based upon the clean airfoil geometry. A 7-bin drop-size distribution was used for each case based upon the NASA IRT icing cloud calibration report [17]. The resulting local collection efficiency and freezing fraction information was then used in the subsequent analysis of the experimental data. The LEWICE prediction results for the local collection efficiency and local freezing fraction are shown in Figures 2 and 3.

The panel code used to predict the local surface pressures was implemented in Mathcad. Figure 4 presents the resulting low-speed pressure coefficient predictions versus surface distance for the two airfoils. For the investigation, the compressible flow corrections were then applied based on Eq. (16).

$$C_P = \frac{C_{P,M=0}}{\sqrt{1 - M_\infty^2}} \tag{16}$$

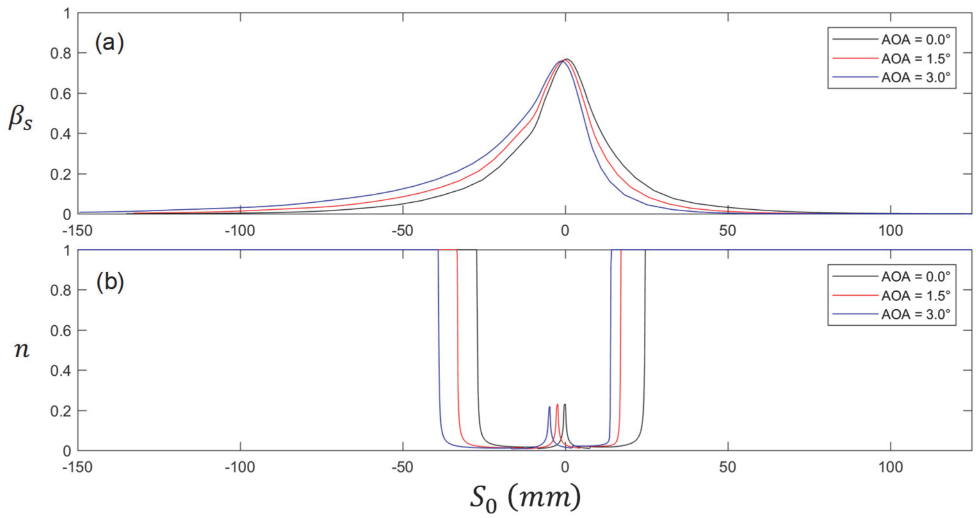

Figure 2. LEWICE Simulations for the NACA 0012 Model in Appendix C (MVD = 29.5 μm) Conditions [11]

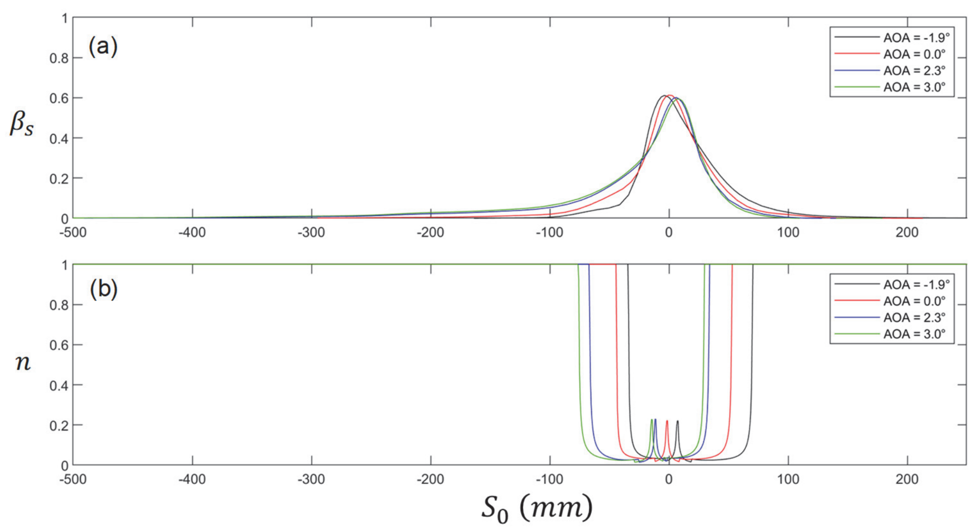

Figure 3. LEWICE Simulations for the HAARP-II Model in Appendix C (MVD = 29.5 μm) Conditions [11]

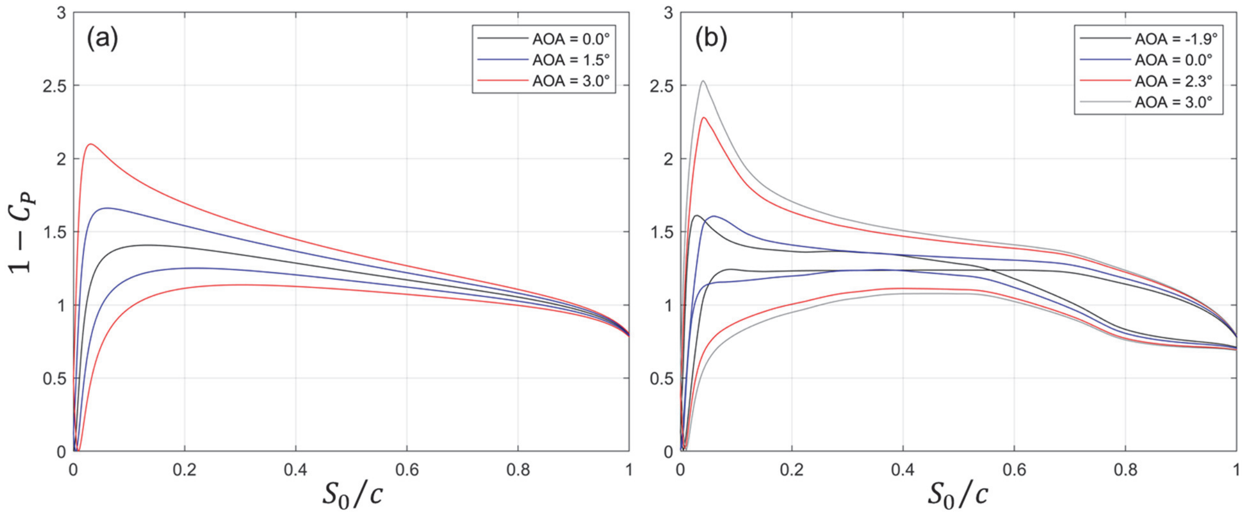

Figure 4. Surface Pressure Coefficient Variations for each Airfoil: (a) NACA 0012 and (b) HAARP-II

For each case listed in Tables 1-4, the roughness measurements were revisited to obtain the pressure coefficient and the collection efficiency at the locations of maximum roughness on each side of the airfoil. Figure 5 presents an example root-mean-square roughness profile using the 110617.09 case for the NACA 0012 at an angle of attack of 3°, where the root-mean roughness, R_q, is defined in Eq. (17).

$$R_{q,\boldsymbol{b_n}} = \left[\frac{1}{J}\sum_{i=1}^{J}\left(N_i - \bar{N}_{\boldsymbol{b_n}}\right)^2\right]^{\frac{1}{2}} \tag{17}$$

Figure 5 demonstrates that the roughness varies along the airfoil surface and exhibits maximums on each side of the airfoil. The local maximum roughness values are not equal because the symmetric airfoil model was in a lifting angle of attack. Using the roughness profiles, the surface distance locations on the top or "suction" surface and on the bottom or "pressure" surface of the airfoil were obtained. Cubic splines of the pressure coefficient results and the local collection efficiency results were found using cubic spline interpolations based on the surface distance locations of the local maximum roughness values.

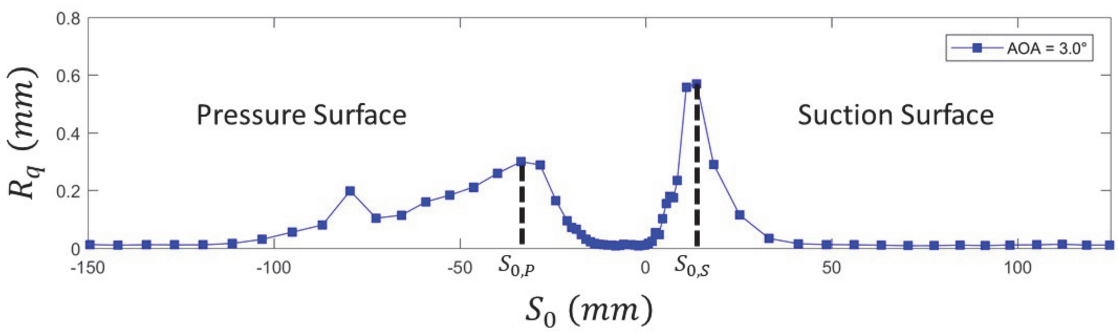

Figure 5. Airfoil Local Maximum Roughness Locations for the 110617.09 Case: NACA 0012 with AOA = 3°

IV. Local Correlation Methodology

In the global airfoil approach to the maximum roughness prediction of Eq. (15), the roughness values were scaled using the stagnation point or stagnation line ideal rime thickness, as defined using Eq. (10). For the local roughness correlation model, the roughness values are made based on the local ideal rime thickness, which is based on the local interpolated collection efficiency as shown in Eq. (18).

$$N_{R,L} = 2r_0 A_c \beta_S \tag{18}$$

In addition to the local pressure and collection efficiency, the local static temperature was investigated for use in correlating the local roughness values. The local static temperature was not found to correlate well with roughness. Interestingly, the static temperatures were found to indicate physics occurring regarding the location of the roughness maximum values along the surface of the airfoil models.

Figure 6 presents local pressure coefficients versus the local supercooling temperature ($T_f - T_{s,L}$) where the maximum roughness values occur. In Figure 6, the dark symbol borders indicate the points are on the pressure surface, while the light symbol borders indicate the points are on the suction surface of the airfoil models. Figure 6 demonstrates that the measurements from the freestream temperature progression cases are grouped along diagonal lines. The diagonal lines start at the subcooling stagnation temperature, ($T_f - T_{0,a}$) and ($T_f - T_{0,b}$) are provided as two examples, and decrease as a result of the compressible flow expressions, thus simply indicating that the measurements occur along the surface of the airfoil. The static temperature progression cases, however, demonstrate the interesting finding that with the exception of two cases, the location of the maximum roughness values is essentially constant for a given angle of attack. The pink dashed lines show the general trend as the stagnation temperature of the cases decreases. For each side of the HAARP-II airfoil, the maximum roughness at high stagnation temperatures starts near the same location as the lower (colder) stagnation temperature cases. However, there is a stagnation temperature case, representing a stagnation point freezing fraction around 0.3, where the location of the maximum roughness shifts forward near the leading edge. These cases are indicated in Figure 6 where the red dashed lines rapidly increase then decrease with increasing stagnation supercooling temperature. The NACA 0012 measurements indicate a similar trend, but the NACA 0012 trend is not as significant as exhibited for the HAARP-II model.

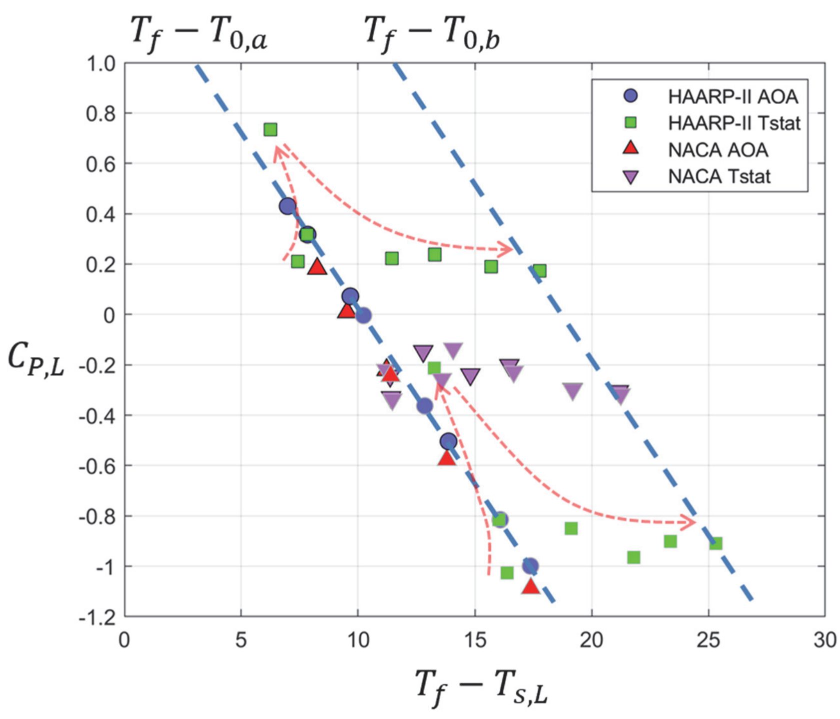

Figure 6. Local Pressure Coefficient at Location of Maximum Roughness versus Local Static Supercooling Temperature

Consequently, the correlation effort focused on relating the maximum roughness on both sides of the NACA 0012 and HAARP-II airfoils scaled by the local ideal-rime thickness ($R_{q,max}/N_{R,L}$) to the local pressure coefficient, $C_{P,L}$, and the stagnation supercooling temperature, $\Delta T_{0S} = T_f - T_0$. A generic regression approach could have been employed to relate the relative roughness to the pressure coefficient and the stagnation supercooling temperature. However, based on the results of McClain et al. [10] and McClain et al. [11], a physics-directed approach was employed based on the expectations that the roughness should vary linearly with pressure coefficient and that the relationship to the stagnation supercooling temperature should follow the trend of $\Delta T_{0S} e^{-\Delta T_{0S}}$.

Figure 7 presents the relative roughness measurements versus the local pressure coefficient for all of the cases in Tables 1-4. Because of the influence of the stagnation temperature, a trend is not immediately apparent in Figure 7. However, the blue-dashed line represents an upper-limit trend for the worst-case stagnation temperature, and consequent worst-case point freezing fraction from Eq. (11) of 0.22. The function for the upper-limit is presented in Eq. (19).

$$\left.\frac{R_{q,max}}{N_{R,L}}\right|_{n_0 \sim 0.22} = 0.7\left(1 - C_{P,L}\right) \tag{19}$$

The correction for stagnation supercooling temperature was then found by dividing the roughness values for the worst-case freezing fraction limit described in Eq. (19). Figure 8 presents the new relative roughness values versus the stagnation supercooling temperature. As demonstrated in Figure 8, significant scatter exists in the worst-case freezing fraction, relative roughness measurements. Correlations were explored that followed the expected trend of $\Delta T_{0S} e^{-\Delta T_{0S}}$ and imposed the constraint that the value of the function should be approximately 1.0 in the stagnation supercooling temperature range that results in a freezing fraction values near 0.22. The blue line shown in Figure 8 is reported in Eq. (20) and represents the median or central prediction for the measurements from Tables 1-4.

$$\frac{R_{q,max}}{N_{R,L}\left(0.7\left(1 - C_{P,L}\right)\right)} = 0.34 + \Delta T_{0S}^{\frac{2}{3}} e^{-\frac{\Delta T_{0S}}{2.25}} \tag{20}$$

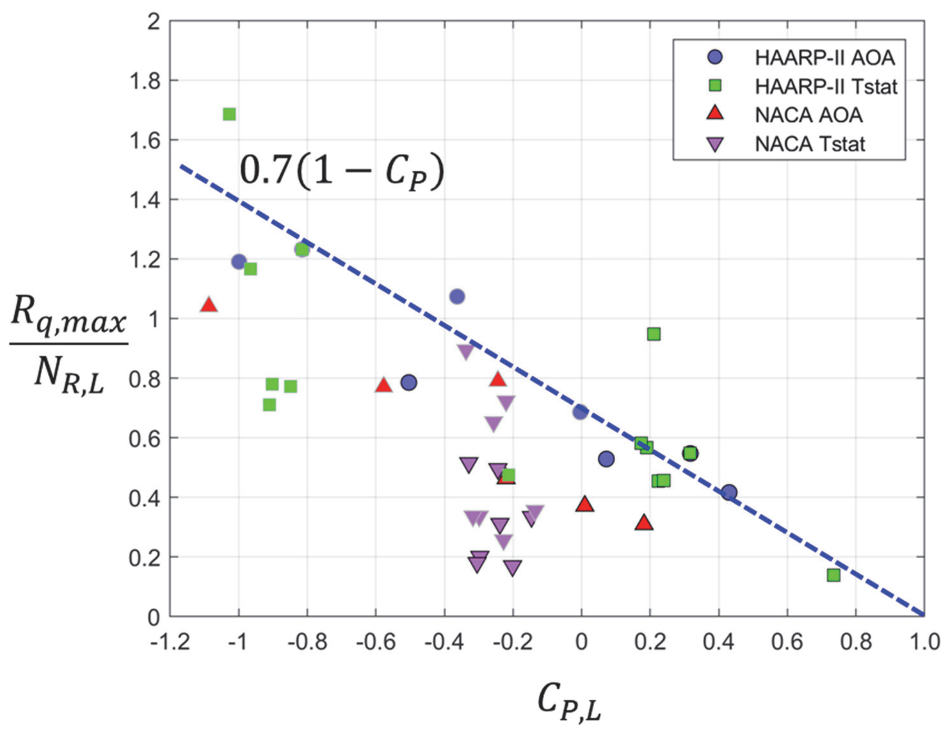

Figure 7. Locally-Scaled RMS Roughness Height versus Local Pressure Coefficient for the Appendix C Cases of McClain et al. [10] and McClain et al. [11]

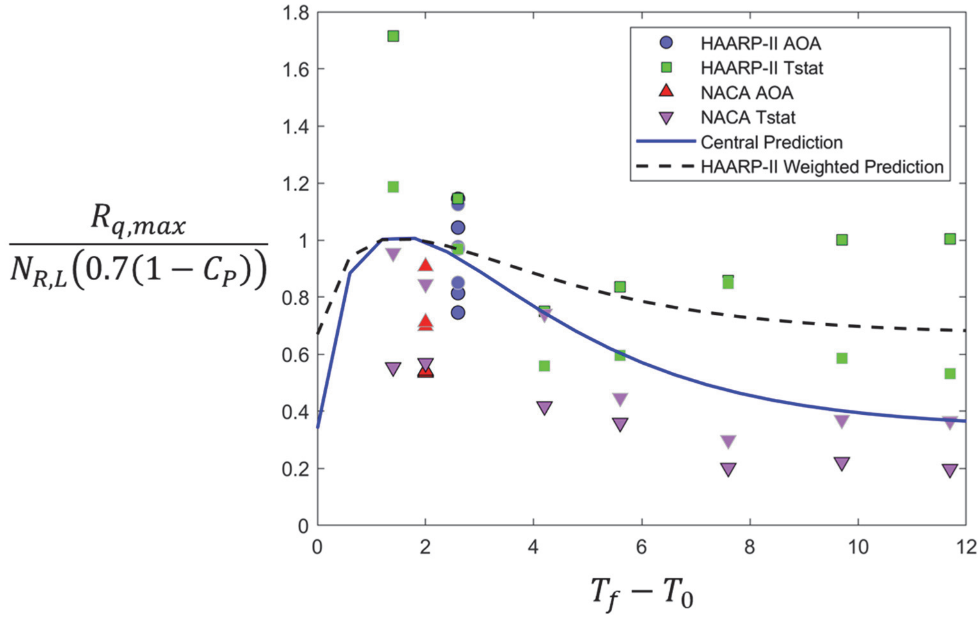

Figure 8. Locally-Scaled RMS Roughness Height versus Stagnation Supercooling Temperature (K) for the Appendix C Cases of McClain et al. [10] and McClain et al. [11]

Inspecting Figure 8, a significant difference is evident between the NACA 0012 cases and the HAARP-II cases especially at the higher values of stagnation supercooling temperature. The cause of the difference between the NACA 0012 cases and the HAARP-II cases is not fully understood. One possibility given the significant difference in size of the airfoil models is that the laser scanning system may have better resolution for the larger HAARP-II roughness than for the much smaller NACA 0012 roughness. However, the investigation of McClain et al. [7] demonstrated similarity between roughness measurements on a 72-in. NACA 0012 model compared to found on the 21-in. model. A second explanation is that, either because of the model or because of the input parameters employed, the LEWICE predictions may not be capturing the correct collection efficiency variations along the HAARP-II surface. As demonstrated in Eq. (18), the local rime thickness used to scale the roughness measurements is directly related to the local collection efficiency. Further, the maximum roughness values occur in regions where the LEWICE predictions indicate that the collection efficiency values are changing significantly along the surface of the airfoil and are significantly less than the maximum collection efficiency near the stagnation point. Uncertainties in the location of the roughness measurement as well as computational uncertainties could lead to differences in local collection efficiency values that significantly skew the scaled roughness measurements on the HAARP-II model.

Since the cause is the difference between the NACA 0012 roughness measurements and the HAARP-II roughness measurements is not understood, a second correlation is provided based on better matching of the HAARP-II roughness measurement. The dashed curve in Figure 8 is reported in Eq. (21).

$$\frac{R_{q,max}}{N_{R,L}\left(0.7\left(1-C_{P,L}\right)\right)} = 0.67 + 0.5\Delta T_{0S}^{\frac{2}{3}} e^{-\frac{\Delta T_{0S}}{2.25}} \tag{21}$$

Eq. (21) more closely matches the HAARP-II measurements and could be used as a "conservative" roughness estimate since the predicted roughness would be larger and be expected to produce higher convection enhancements.

Eqns. (20) and (21) are then transformed for the prediction of the local roughness based on the local pressure coefficients and the stagnation supercooling temperature. Eq. (22) is provided for the "median" prediction, and Eq. (23) is provided for the conservative or "HAARP-II weighted" prediction of the relative roughness.

$$\left.\frac{R_{q,max}}{N_{R,L}}\right|_{Med} = \left(0.7(1-C_P)\right)\left(0.34 + \Delta T_{0S}^{\frac{2}{3}} e^{-\frac{\Delta T_{0S}}{2.25}}\right) \tag{22}$$

$$\left.\frac{R_{q,max}}{N_{R,L}}\right|_{H-II} = \big(0.7(1-C_P)\big)\left(0.67 + 0.5\Delta T_{0S}^{\frac{2}{3}} e^{-\frac{\Delta T_{0S}}{2.25}}\right) \tag{23}$$

Figure 9 presents the three-dimensional median prediction surface of Eq. (22) for the local relative roughness versus the local pressure coefficient and the stagnation supercooling temperature. The measured relative roughness values for the cases of Tables 1-4 are included in Figure 9 and are connected to their respective predictions using vertical gray lines. The data and the difference lines demonstrate that the trends of the data are captured, but deviations are present. The root-mean-square error in the relative roughness predictions was calculated using Eq. (24).

$$E_{RMS} = \left[\frac{1}{N}\sum\left(\left.\frac{R_{q,max}}{N_{R,L}}\right|_{meas} - \left.\frac{R_{q,max}}{N_{R,L}}\right|_{Pred}\right)^2\right]^{\frac{1}{2}} \tag{24}$$

The root-mean-square error for the "median" correlation is 23%. In addition to the prior issue noted regarding predictions of collection efficiency, the Lagrangian or stochastic nature of the ice accretion process is also causing scatter in the measurement. Additionally, the local pressure coefficient is expected to vary with other parameters such as the local fluid shear stress or the local liquid film thickness. Given, the complexities of the ice accretion process and the many parameters that influence the roughness formation process, the root-mean-square error is reasonable.

Figure 10 presents the three-dimensional conservative prediction surface of Eq. (23) for the local relative roughness versus the local pressure coefficient and the stagnation supercooling temperature. Comparing Figure 10 to Figure 9, the difference bars between the predictions and the HAARP-II measurements is reduced, while the difference between the prediction and the NACA 0012 measurements is significantly increased. Still, the root-mean-square error for the conservative or HAARP-II biased correlation is 26%, but the root-mean-square error for just the HAARP-II cases is 17%.

V. Application of Correlation to Specific Cases

While the correlations of Eq. (22) and (23) were developed using the maximum roughness measurements along each iced airfoil condition, the correlations are intended to be applied locally. In this section, the correlation are applied to specific cases from the studies of McClain et al. [10] and McClain et al. [11] to investigate performance of the local roughness model when used to make local predictions along a surface.

Figures 11 and 12 present the comparison of the measured and predicted roughness for the 110617.09 case from Table 3 for a 21-in. NACA 0012 airfoil model. Figure 11 presents the variations in measured and predicted RMS roughness along the model at 3° AOA and $n_0 = 0.22$. The red curve and data are the measured Rq values along the 110617.09 point cloud surface, and the blue curve is the prediction from the median prediction of Eq. (22). Figure 11 demonstrates that the median correlation is slightly higher than the measurements for the NACA 0012 but tracks the measured roughness values outside the region of the maximum roughness values. Inside the locations of the maximum local roughness near the stagnation point on the airfoils surface, the local median correlation significantly over estimates the roughness. Revisiting Figure 2(b), the LEWICE predictions indicate that the freezing fractions are near zero in the stagnation region between the two local roughness maximums and then rapidly approach values of 1.0 near the locations of maximum roughness.

The maximum combined cross-section (MCCS) was introduced by Broeren et al. [18] and describes the extent of the point cloud away from the clean airfoil at a given surface location. Based on the self-organizing map approach for the roughness characterization used by McClain et al. [10 and 11], the predicted MCCS shape is calculated using 3.09Rq, which is the 99% roughness height prediction based on Gaussian statistics, projected from the measured mean ice shape surface. Figure 12(a) shows a projected view of the predicted MCCS using the correlation if Eq. (18) compared to the measured MCCS. In Figure 12(a), the red curve represents the measured MCCS, and the purple curve represents the predicted MCCS profile using the median prediction of Eq. (22). Figure 12(a) demonstrates the same information as Figure 11, but in airfoil coordinates.

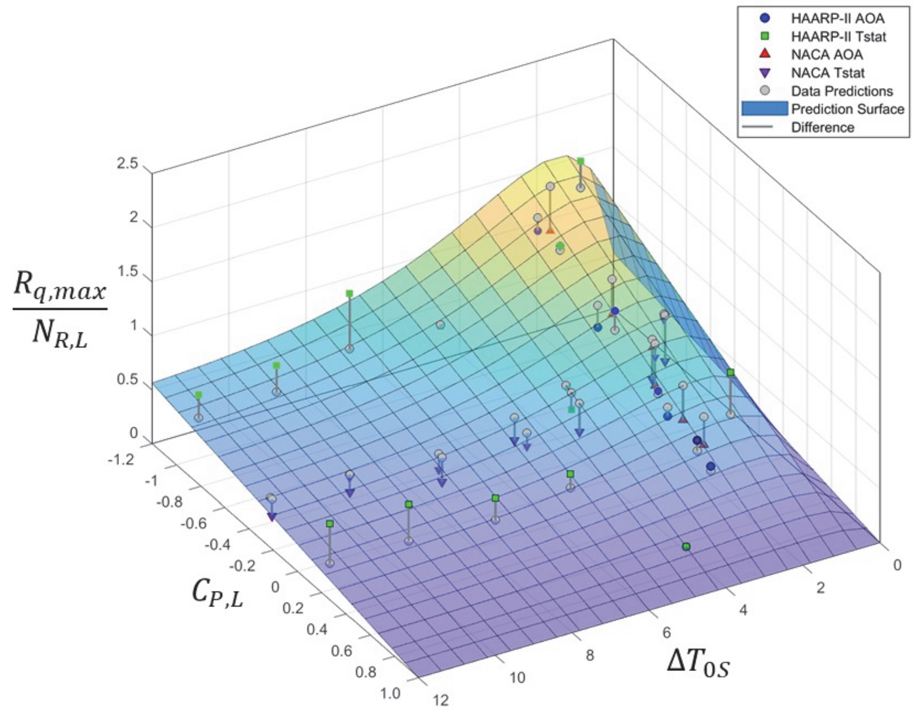

Figure 9. Three-Dimensional Surface Presentation of Scaled Roughness Height Measurements and Predictions versus Pressure Coefficient and Stagnation Supercooling Temperature using the Median Prediction of Eq. (22)

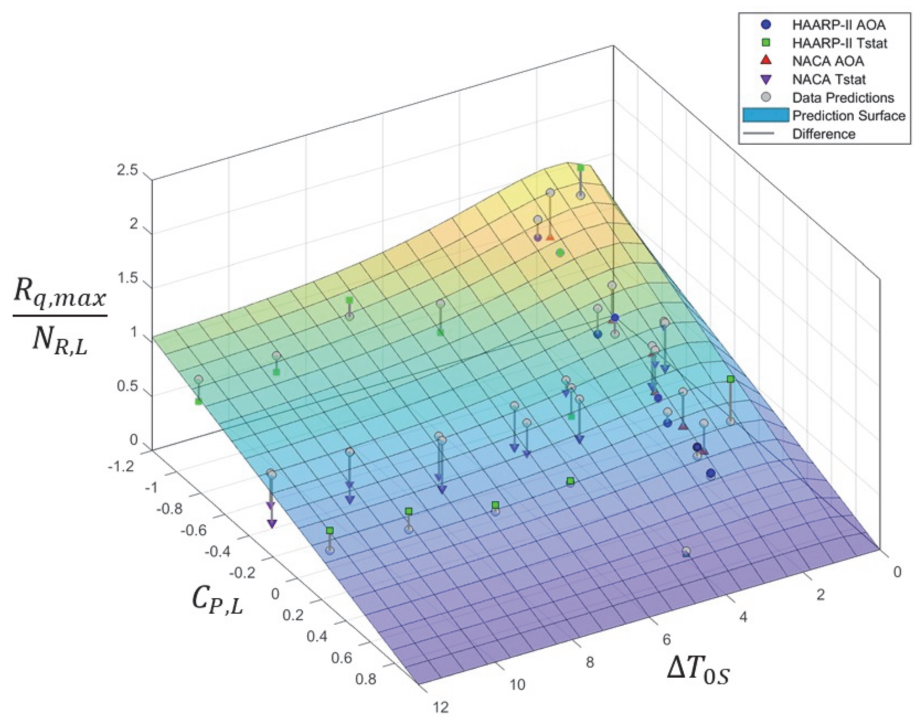

Figure 10. Three-Dimensional Surface Presentation of Scaled Roughness Height Measurements and Predictions versus Pressure Coefficient and Stagnation Supercooling Temperature using the HAARP-II Weighted Prediction of Eq. (23)

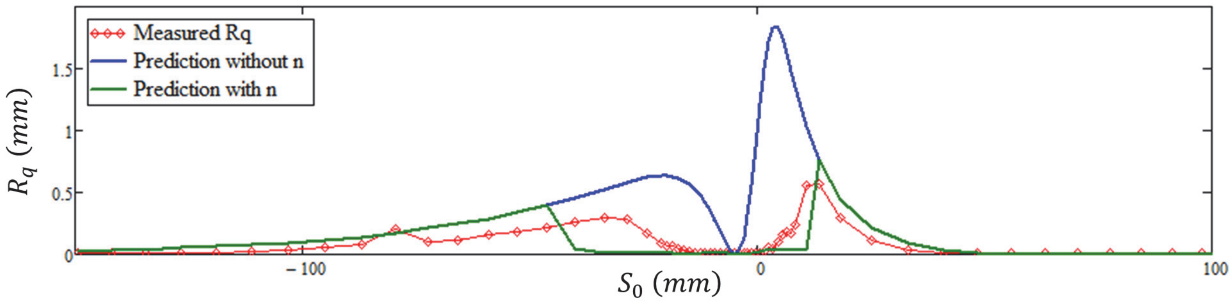

Figure 11. Predicted and Measured RMS Roughness Variation along a 21-in. NACA 0012 in Appendix C Conditions at 3° AOA and n_0 = 0.22 (Case 110617.09)

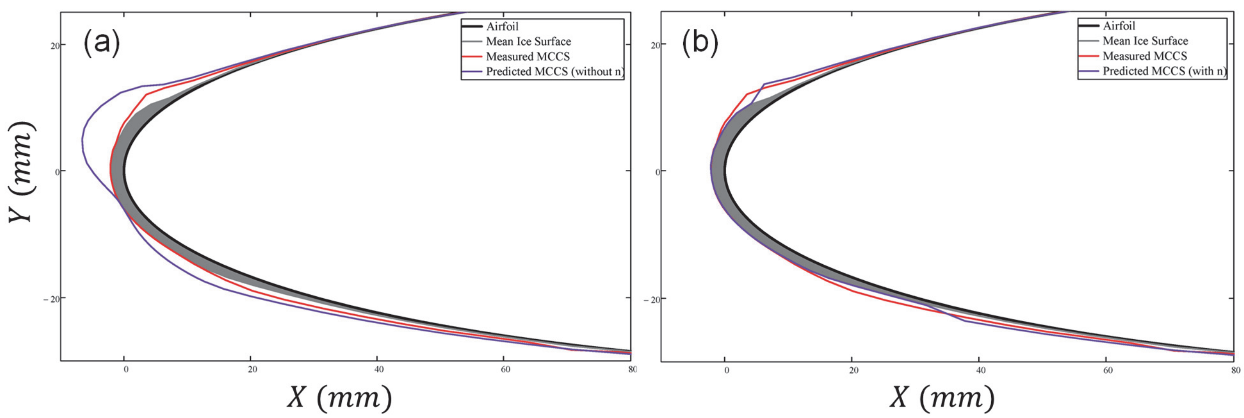

Figure 12. Measured and Predicted MCCS Projected Shapes for a 21-in. NACA 0012 in Appendix C Conditions at 3° AOA and n_0 = 0.22 (Case 110617.09): (a) Without Freezing Fraction Correction, (b) With Freezing fraction Correction

Figures 13 and 14 present the same comparisons for the 60-in. HAARP-II airfoil model at 2.3° AOA and n_0 = 0.22 (Case 012517.03) and employing the median correlation of Eq. (22). Recalling Figure 8, both stagnation supercooling corrections are near 1.0 at temperatures resulting in freezing fractions near 0.22. As such, there is only a 3% difference between the HAARP-II weighted correlation and the median correlation. Figure 13 and Figure 14(a) again show that outside the locations of local maximum roughness, the correlation predictions follow the measured roughness. Additionally, at the locations of local maximum roughness, the predicted values are very close to the measured roughness values. However, inside the locations of maximum roughness near the stagnation point, the roughness values are significantly overestimated.

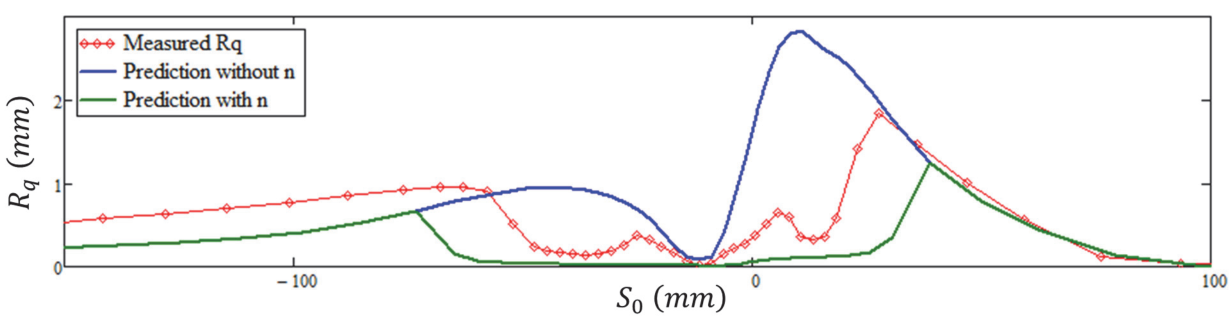

Figure 13. Predicted and Measured RMS Roughness Variation along a 60-in. HAARP-II in Appendix C Conditions at 2.3° AOA and n_0 = 0.22 (Case 012517.03)

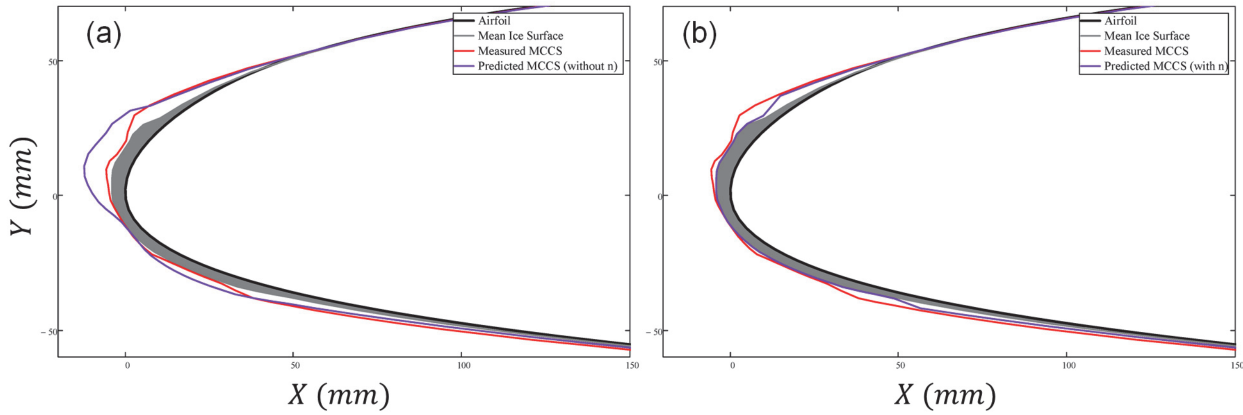

Figure 14. Measured and Predicted MCCS Projected Shapes for a 60-in. HAARP-II in Appendix C Conditions at 3° AOA and n_0 = 0.22 (Case 012517.03): (a) Without Freezing Fraction Correction, (b) With Freezing fraction Correction

Figures 11-14 and the lack of agreement in the glaze region between the local roughness maximums demonstrate that the local freezing fraction must be considered in the local roughness prediction model. Revisiting figures 2(b) and 3(b), the freezing fractions predicted using LEWICE are near 0.0 then increase abruptly near the location of maximum roughness. Thus, median correlation and the HAARP-II weighted correlations are updated to include the freezing fraction as shown in Eqns. (25) and (26).

$$\left.\frac{R_q}{N_{R,L}}\right|_{Med} = n\big(0.7(1-C_P)\big)\left(0.34 + \Delta T_{0S}^{\frac{2}{3}} e^{-\frac{\Delta T_{0S}}{2.25}}\right) \tag{25}$$

$$\left.\frac{R_q}{N_{R,L}}\right|_{H-II} = n\big(0.7(1-C_P)\big)\left(0.67 + 0.5\Delta T_{0S}^{\frac{2}{3}} e^{-\frac{\Delta T_{0S}}{2.25}}\right) \tag{26}$$

The green curves in Figures 11 and 13 present the updated predictions of the roughness R_q values along the surfaces of the NACA 0012 and HAARP-II airfoils for similar conditions. Likewise, Figures 12(b) and 14(b) present the updated MCCS profiles using the freezing fraction modifications to the local correlations. Figures 11-14 demonstrate that including the freezing fraction has the potential to capture the locations of the maximum roughness. As with the collection efficiency employed in the However, Figures 11-14 also demonstrate that now the roughness is underestimated in the glaze region near the stagnation points of the airfoils.

VI. Reflection on Correlation and Icing Physics

Revisiting the median prediction of Eq. (25), substituting for the local ideal rime ice thickness and substituting for the accumulation parameter results Eq. (27), which expands the local root-mean-square roughness prediction in terms of cloud, airspeed, and thermodynamic properties.

$$R_q = \underbrace{\frac{LWC \cdot V \cdot \Delta t_s}{\rho_{ice}} \beta_S}_{\text{Local ideal mass accreted based on collection and event time}} \underbrace{\big(0.7(1-C_P)\big)}_{\text{Local surface pressure correction}} \underbrace{n\left(0.34 + \Delta T_{0S}^{\frac{2}{3}} e^{-\frac{\Delta T_{0S}}{2.25}}\right)}_{\text{Stagnation temperature and local energy balance correction}} \tag{27}$$

Eq. (27) demonstrates that the forms of either the median correlation or the HAARP-II weighted correlation can be grouped into three terms: 1) a term that includes the ideal mass accreted based on collection efficiency and icing event time, 2) a term that corrects for the local surface pressures, and 3) a term that includes the total temperature as well as the local thermodynamic state based on the freezing fraction. Other factors such as the local shear and the liquid film thickness are expected to influence the roughness formation, especially in the glaze region near the freezing fraction. However, the terms captured in Eq. (27) are reasonable and intuitive in their influence on the local roughness evolution.

Most roughness, turbulence, and convective enhancement models include the equivalent sand-grain roughness as opposed to the root-mean-square roughness of Eq. (27). The correlation of Flack and Schultz [19] is recommended for converting the R_q values to k_s values. However, the correlation requires a value of the statistical skewness. For a measured ice shape, the skewness can be easily determined. Without direct knowledge of the skewness, such as during a design calculation employing the model of Eq. (27), the authors recommend simply assuming a Gaussian surface distribution, which would imply a skewness value of 0.0.

Another issue that must be addressed in future research is the question of when does the roughness stop changing or becomes “frozen” during an ice accretion event. In LEWICE, the roughness is a constant and assumed to be the maximum roughness along the surface at the instant the ice shape transitions from “roughness on an airfoil” to a “fully two-dimensional or three-dimensional ice shape.” Typically, once the ice shape becomes two-dimensional or three-dimensional, the roughness is considered to be “frozen.” Determining the validity of this assumption and its impact on the convection enhancement prediction requires future investigation.

Finally, the inclusion of the freezing fraction in the roughness prediction correlations highlights a fundamental complexity associated with ice accretion prediction and ice roughness prediction. Conceptually, the reason for developing a roughness correlation is to predict convective heat transfer enhancement. The convective heat transfer enhancement is required to predict freezing fraction, and the freezing fraction determines how much mass is accreted on the surface at the given time step. However, the freezing fraction is required to predict the roughness. The circular dependencies are depicted in Figure 15.

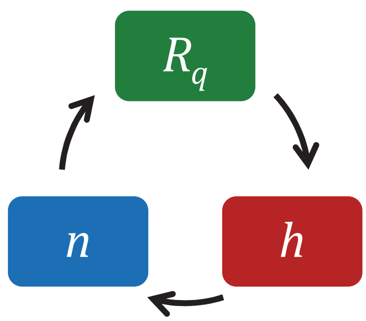

Figure 15. Cyclic Dependency of Roughness, Convective Enhancement, and Freezing Fraction that Occurs on an Ice Accretion Surface

In LEWICE, the circular issues are resolved by capturing the correct maximum roughness at the critical point during an icing event where the ice shape transitions from “roughness on an airfoil” to an “airfoil with a fully two or three-dimensional ice shape” [1,2]. The challenge for future icing models and ice accretion codes is to identify how and at what step in the cycle depicted in Figure 15 to accurately capture the freezing fraction and subsequent mass accretion on the simulated surface.

Many options other than the LEWICE approach are available to break into the roughness prediction cycle of Figure 15, but many of the options require considerable computational costs. Based on the approach of two separate codes: one code for the Navier-Stokes flow solution the droplet collection efficiency and another code for icing physics modeling, one approach to entering the cycle is to perform a first CFD simulation for a smooth model. The local pressure coefficient and collection efficiency would then be used to predict the roughness along the model excluding the freezing fraction. Because turbulence models that handle roughness variations along a surface are not widely available or validated, the surface would then be queried to determine the maximum roughness predicted along a model surface or at the critical laminar-turbulent transition location along a model. The maximum or critical roughness value would then be employed in a CFD simulation using a validated roughness model to predict the rough skin friction coefficients and the rough convection coefficients along the model surface. Alternatively, if a convection prediction model is not validated, the approach of Kays and Crawford [20, 1] could be used based on the local sand-grain roughness and the rough skin friction coefficient. The heat transfer coefficients along the model surface would then be passed to the icing physics solver for the accretion prediction over a time step. Future investigations of this potential roughness and convective enhancement implementation and other approaches to entering the cyclic roughness definition are recommended.

VII. Conclusion

The maximum roughness measurements of McClain et al. [10] and McClain et al. [11] were revisited to develop and investigate a local roughness correlation approach. Two correlations are presented representing 1) a “median” prediction or 2) a conservative prediction which was weighted more heavily by the roughness measurements on the HAARP-II airfoil model. The correlations express the root-mean-square roughness, scaled by the local ideal rime thickness, in terms of 1) a local pressure coefficient correction term and 2) a stagnation supercooling temperature correction term. Following comparison to example ice shapes on a NACA 0012 model and on a HAARP-II model, the local freezing fraction was also included in the correlations.

The root-mean-square error in the predictions of relative roughness is 23% for the median correlation and 26% for the HAARP-II weighted correlation. The scatter of the data about the correlations is caused by the facts that 1) the ice accretion is stochastic (Lagrangian) and 2) other parameters such as local shear and local liquid film thickness, which are suspected to influence the local roughness, are not included in the correlation.

When the median correlation was applied to example ice shapes for local roughness prediction, the correlation captured the magnitudes and trends of the local roughness measurements outside the glazing-stagnation region. Inside the glaze-stagnation region, the roughness is overestimated when the local freezing fraction is not considered and underestimated when the roughness correlation is multiplied by the value of the local freezing fraction.

In addition to the effects of the local shear and local liquid film thickness, the limiting roughness values when an ice accretion transitions from “roughness on an airfoil” to a fully two or three-dimensional ice shape are not currently known. Finally, since the roughness correlation requires knowledge of the local freezing fraction, the cyclic nature of the roughness prediction was discussed. Future research is required to identify how to enter the cyclic process of roughness, convection enhancement, and freezing fraction to predict ice accretion on aircraft surfaces using future ice accretion codes.

Acknowledgments

The efforts reported in this paper were supported as part of NASA Collaborative Agreement No. NNX16AN32A through the Advanced Air Transport Technology (AATT) program. The authors thank Mr. Richard E. Kreeger, Mrs. Laura King-Steen, Mr. Quentin Schwinn, Ms. Jordan Salkin, and Dr. Sam Lee for their assistance with the study. Any opinions presented in this paper are those of the authors and do not reflect any official or unofficial views of NASA or the United States government.

References

[1]Wright, W., “User’s Manual for LEWICE Version 3.2,” NASA/CR—2008-214255, Nov. 2008.

[2]Shannon, T. and McClain, S.T., (2020), "An Assessment of LEWICE Roughness and Convection Enhancement Models," *SAE Int. J. Adv. and Curr. Prac. in Mobility*, 2(1):128-139, https://doi.org/10.4271/2019-01-1977.

[3]Kays, W.M, and Crawford, M.E., (1993), Convective Heat and Mass Transfer, McGraw-Hill, New York, 3rd edition.

[4]McClain, S.T., Reed, D., Vargas, M., Kreeger, R.E., and Tsao, J.-C.,, (2014), “Ice roughness in Short Duration SLD Icing Events,” Presented at the 6th AIAA Atmospheric and Space Environments Conference, June 16-20, Atlanta, GA, AIAA-2014-2330.

[5]McClain, S.T., Vargas, M., Kreeger, R.E., and Tsao, J.-C., (2015), “A Reevaluation of Appendix C Ice Roughness Using Laser Scanning,” SAE 2015 International Conference on Icing of Aircraft, Engines, and Structures, June 22-25, Prague, Czech Republic, SAE2015-01-2098.

[6]Anderson, D. N., Hentschel, D. B., and Ruff, G. A., (1998), “Measurement and Correlation of Ice Accretion Roughness,” NASA CR—2003-211823.

[7]McClain, S.T., Vargas, M., and Tsao, J.-C., (2016), “Characterization of Ice Roughness Variations in Scaled Glaze Icing Conditions,” 8th AIAA Atmospheric and Space Environments Conference, June 13-17, Washington, DC, AIAA-2016-3592.

[8]McClain, S.T., Vargas, M., and Tsao, J.-C., (2017), “Ice Roughness and Thickness Evolution on a Swept NACA 0012 Airfoil,” 9th AIAA Atmospheric and Space Environments Conference, June 5-9, Denver, CO, AIAA-2017-3592.

[9]McClain, S.T., Vargas, M., Tsao, J.-C., and Broeren, A.P., (2018), "Ice Roughness and Thickness Evolution on a Business Jet Airfoil," 10th AIAA Atmospheric and Space Environments Conference, June 25-29, Atlanta, GA, AIAA-2018-3014.

[10]McClain, S.T., Vargas, M., Tsao, J.-C., and Broeren, A., (2020), "Influence of Freestream Temperature on Ice Accretion Roughness," *SAE Int. J. Adv. and Curr. Prac. in Mobility*, 2(1):227-237, https://doi.org/10.4271/2019-01-1993.

[11]McClain, S.T., Vargas, M., Tsao, J.-C., Broeren, A.P., (2020), "Influence of Airfoil Angle of Attack on Ice Accretion Roughness," 2020 AIAA Aviation Forum, Reno, NV, June 15-19, AIAA-2020-2807.

[12]Papadakis, M., Wong, S.-H., Yeong, H.-W., Wong, S.-C., and Vu, G.T., (2008), "Icing Tunnel Experiments with a Hot Air Anti-Icing System," AIAA-2008-444.

[13]Drela, M., (2011), "Development of the D8 Transport Configuration," 29th AIAA Applied Aerodynamics Conference, 27-30 June, Honolulu, HI, AIAA-2011-3970.

[14]Anderson, D.N, and Tsao, J.-C., (2005), "Overview of Icing Physics Relevant to Scaling," NASA/CR-2005-213851.

[15]Ruff, G.A., 1986, Analysis and Verification of the Icing Scaling Equations, AEDC–TR–85–30, vol. 1 (Rev), March 1986.

[16]Langmuir, I. and Blodgett, K. B. "A Mathematical Investigation of Water Droplet Trajectories," Army Air Forces Technical Report No. 5418, February 1946.

[17]Steen, L.E., Ide, R.F., Van Zante, J.F., Acosta, W.J., "NASA Glenn Icing Research Tunnel: 2014 and 2015 Cloud Calibration Procedures and Results," NASA/TM—2015-218758, May 2015.

[18]Broeren, A.P., Potapczuk, M.G., Riley, J.T., Villedieu, P., Moens, F., and Bragg, M.B., (2013), "Swept-Wing Ice Accretion Characterization and Aerodynamics," AIAA Paper 2013-2824, June 2013, also NASA/TM—2013-216555, Sept., doi: 10.2514/6.2013-2824.

[19]Flack, K. A., and Schultz, M. P., (2010), "Review of Hydraulic Roughness Scales in the Fully Rough Regime," Journal of Fluids Engineering, 132(4), p. 041203.

[20]Kays, W.M, and Crawford, M.E., (1993), Convective Heat and Mass Transfer, McGraw-Hill, New York, 3rd edition.